REPORT DOCUMENTATION PAGE

Form Approved
OMB No. 0704-0188

1. REPORT DATE *(DD-MM-YYYY)*	**2. REPORT TYPE**	**3. DATES COVERED** *(From - To)*
December 2013	Technical Paper	December 2013- January 2014

4. TITLE AND SUBTITLE
Computational Study of Combustion Dynamics in a Single-Element Lean Direct Injection Gas Turbine Combustor

5a. CONTRACT NUMBER
In-House

5b. GRANT NUMBER

5c. PROGRAM ELEMENT NUMBER

6. AUTHOR(S)
Huang, C., Yoon, C., Gejji, R., Anderson, W. and Sankaran, V.

5d. PROJECT NUMBER

5e. TASK NUMBER

5f. WORK UNIT NUMBER
Q12M

7. PERFORMING ORGANIZATION NAME(S) AND ADDRESS(ES)

Air Force Research Laboratory (AFMC)
AFRL/RQR
5 Pollux Drive.
Edwards AFB CA 93524-7048

8. PERFORMING ORGANIZATION REPORT NO.

9. SPONSORING / MONITORING AGENCY NAME(S) AND ADDRESS(ES)
Air Force Research Laboratory (AFMC)
AFRL/RQR
5 Pollux Drive
Edwards AFB CA 93524-7048

10. SPONSOR/MONITOR'S ACRONYM(S)

11. SPONSOR/MONITOR'S REPORT NUMBER(S)
AFRL-RQ-ED-TP-2013-283

12. DISTRIBUTION / AVAILABILITY STATEMENT
Distribution A: Approved for Public Release; Distribution Unlimited. PA#13564

13. SUPPLEMENTARY NOTES
Conference Paper for the AIAA Science and Technology Forum and Exposition, National Harbor, MD, 13-17 Jan 2014.

14. ABSTRACT

Simulations of self-excited combustion instabilities in a model configuration of a lean direct injection (LDI) gas turbine combustor were performed and investigated with different operating conditions (air temperature and equivalence ratio). Concurrently, experimental data were obtained at the same conditions in a well-instrumented test combustor with the same configuration to validate the simulation results. The simulations are used to investigate the coupling between the acoustic and heat release modes and the important flow dynamics to understand the physics that lead to combustion instabilities in the LDI combustor. A Precessing Vortex Core (PVC) hydrodynamic instability was found to be significant in driving spray and flame responses. Detailed and systematic studies of the PVC instability are also performed using non-reacting simulations of an acoustically-open combustor to minimize the acoustic and combustion effects on the flow field.

15. SUBJECT TERMS

16. SECURITY CLASSIFICATION OF:			**17. LIMITATION OF ABSTRACT**	**18. NUMBER OF PAGES**	**19a. NAME OF RESPONSIBLE PERSON**
					Venkateswaran Sankaran
a. REPORT	**b. ABSTRACT**	**c. THIS PAGE**	SAR	19	**19b. TELEPHONE NO** *(include area code)*
Unclassified	**Unclassified**	**Unclassified**			661-525-5534

Standard Form 298 (Rev. 8-98)
Prescribed by ANSI Std. 239.18

Computational Study of Combustion Dynamics in a Single-Element Lean Direct Injection Gas Turbine Combustor

Cheng Huang[1], Changjin Yoon[2], Rohan Gejji[3] and William E. Anderson[4]
Purdue University, West Lafayette, IN, 47907

and

Venkateswaran Sankaran[5]
Air Force Research Laboratory (AFRL), Edwards AFB, CA, 93524

Simulations of self-excited combustion instabilities in a model configuration of a lean direct injection (LDI) gas turbine combustor were performed and investigated with different operating conditions (air temperature and equivalence ratio). Concurrently, experimental data were obtained at the same conditions in a well-instrumented test combustor with the same configuration to validate the simulation results. The simulations are used to investigate the coupling between the acoustic and heat release modes and the important flow dynamics to understand the physics that lead to combustion instabilities in the LDI combustor. A Precessing Vortex Core (PVC) hydrodynamic instability was found to be significant in driving spray and flame responses. Detailed and systematic studies of the PVC instability are also performed using non-reacting simulations of an acoustically-open combustor to minimize the acoustic and combustion effects on the flow field.

I. Introduction

Lean direct injection is a promising combustor concept where liquid fuel is injected and mixed with air rapidly in a short distance. In the configuration used here, a subsonic venturi is used in combination with an air swirler and pressure atomizer to provide highly inertial forces for atomization and mixing. It was developed as an alternative to Lean Prevaporized Premixed (LPP) combustion for improved low NOx emissions that eliminates issues encountered in LPP combustion such as auto-ignition and flash-back. Yi and Santavicca's experimental study indicated similarity of flame spectra in an LDI combustor to those in observed in lean premixed gaseous combustion. [1] However, as with other lean-burning combustors, the LDI combustor can be susceptible to self-excited combustion instabilities as the equivalence ratio approaches fuel lean conditions. Under such conditions, the combustion response can be coupled with the acoustic fluctuations to sustain combustion instabilities in the combustor.

In the experimental study of Cohen et al., [2] oscillating levels of pressure at longitudinal acoustic frequencies were reported within 3% of the mean chamber pressure. Concurrent experimental and computational studies of an unstable LDI configuration are being performed at Purdue University starting in 2011. This work is aimed in part at validating high-fidelity simulations using the benchmark experiments and in part to elucidate the underlying physical phenomena that govern the occurrence of combustion instabilities. Once validated, the simulation results can be used with confidence to design stable LDI configurations.

Preliminary studies and comparisons between experiment and simulation have been done by Yoon et al. [3] Specifically, inlet geometry effects were investigated to minimize the effect of the inlet on downstream hydrodynamic unsteadiness. Parametric assessments were performed using two--dimensional axisymmetric

[1] Graduate Research Assistant, School of Mechanical Engineering and Student Member AIAA.
[2] Combustion Dynamics Research Engineer, Combustion Dynamics and Diagnostics Lab, GE Global Research Center and Member AIAA.
[3] Graduate Research Assistant, School of Mechanical Engineering and Student Member AIAA.
[4] Professor, School of Aeronautics and Astronautics and Associate Fellow AIAA.
[5] Senior Scientist, Rocket Propulsion Division and Senior Member AIAA.

simulations. The simulations were performed using specified log-normal distributed drop injection both with and without Reitz's breakup model [4,5] to describe the secondary atomization. Different equivalence ratios were used to compare with experiment data. Additionally, details of the fuel spray modeling effects on the combustion dynamics predictions have also been studied in Ref 6. The spray characteristics (spray angle, drop size distribution etc.) were compared between the experimental measurements and simulation results at atmospheric pressure conditions in an unconfined geometry. Three fuel spray injection models, viz., Log Normal Distributed Drop Injection Model, Single Drop Injection Model and Hollow Cone Injection Model, have been evaluated for their capabilities of predicting combustion instability and matching experiment results. An overview of the modeling effects is summarized in part B of section III. More recently, an enhanced hybrid fuel spray model has been developed to provide more sophisticated descriptions of spray.[7] The hybrid model combines the Linear Instability Sheet Atomization (LISA) model for primary atomization with the Taylor Analogy Breakup (TAB), Kelvin-Helmholtz, and Rayleigh-Taylor models for secondary atomization. Again, a reduced geometry of an unconfined configuration was used to perform detailed studies of hydrodynamic effects on acoustics and combustion. Details of the enhanced model are given in part D of section III.

The present paper is focused on applying the enhanced hybrid spray model developed in Ref 7 to more detailed investigations of the acoustic modes and coupling phenomena in the LDI combustor configuration. As an initial step, non-reacting flow simulations with the reduced geometry are used to illustrate the important hydrodynamic modes (PVC and spinning modes) present in configuration. Next, comparisons of the effects of different fuel spray models on the predictions of combustion instability are summarized. The remainder of the paper is focused on parametric studies of the combustion instabilities for different equivalence ratios and fuel injector locations. Comparisons of the computational and experimental results are carried out using the amplitudes and frequencies of the dominant acoustic modes. Dynamic Mode Decomposition (DMD) is used as a diagnostic tool to investigate mode shapes at the dominant frequencies (either acoustically-related or hydrodynamic-driven) to understand the couplings between acoustics, combustion and hydrodynamics. These results allow us to hypothesize the key physics underlying the cyclic phenomena in the combustor.

II. Computational Model and Diagnostic Tool

A. Computational Framework (GEMS)

The computational platform for the present simulations is our in-house code, GEMS (General Equation and Mesh Solver). [8-11] GEMS is a fully unstructured, density-based finite volume solver with a second-order numerical scheme and an implicit, dual time procedure for time-accuracy. The capabilities of the code for capturing combustion dynamics and estimating instabilities have been successfully demonstrated for rocket engines combustors.[12, 13] GEMS solves the Navier-Stokes equations in Detached Eddy Simulation (DES) mode along the continuity, energy and species equation described below.

$$\frac{\partial Q}{\partial t} + \nabla \cdot \left(F - F_v \right) = S \tag{1}$$

where the conservative variables, Q, inviscid and viscous flux vectors, F and F_v, and source term vector, S, are given by

$$Q = \begin{pmatrix} \rho \\ \rho \mathbf{Y} \\ \rho \mathbf{V} \\ \rho h^0 - p \\ \rho \mathbf{K} \end{pmatrix}, \quad F = \begin{pmatrix} \rho \mathbf{V}^T \\ \rho \mathbf{Y} \mathbf{V}^T \\ \rho \mathbf{V} \mathbf{V}^T + p\bar{I} \\ \rho h^0 \mathbf{V}^T \\ \rho \mathbf{K} \mathbf{V}^T \end{pmatrix}, \quad F_v = \begin{pmatrix} 0 \\ \rho D \nabla \mathbf{Y} \\ \bar{\tau} \\ \bar{\tau} \cdot \mathbf{V} - q \\ \mu_K \nabla \mathbf{K} \end{pmatrix} \quad \text{and} \quad S = \begin{pmatrix} 0 \\ \dot{\omega} \\ 0 \\ 0 \\ s_K \end{pmatrix} + S_L \tag{2}$$

The quantities; ρ, $\mathbf{V}$ and p represent the density, velocity vector and pressure, respectively; h^0 is the stagnation enthalpy and $\mathbf{Y}$ is a species mass fraction vector; $\mathbf{K}$ represents the turbulence variable vector which includes turbulence kinetic energy and specific dissipation, k and w; In the viscous flux, D is the molecular diffusion coefficient; τ is the stress tensor and q is the heat flux; w and s_K are the reaction rate and sources of the turbulence transport equations, respectively. A pseudo-time term expressed in terms of the primitive variables, $Q_p = \begin{bmatrix} p & \mathbf{Y} & \mathbf{V} & T & \mathbf{K} \end{bmatrix}^T$ and a preconditioning matrix, Γ, is added to Eq. (1), so that the equation becomes:

$$\Gamma \frac{\partial Q_p}{\partial \tau} + \frac{\partial Q}{\partial \tau} + \nabla \cdot \left(F - F_v \right) = 0 \tag{3}$$

The matrix, Γ, is chosen to control the artificial dissipation in the spatial discretization and the convergence of the pseudo-time iterations. The preconditioning matrix, Γ, in the pseudo time term in Eq. (3), is defined by starting from the Jacobian of the conservative variables with respect to the primitive variables, $\partial Q / \partial Q_p$, as shown below:

$$\Gamma = \begin{pmatrix} \rho_p' & \rho_{\mathbf{Y}} & 0 & \rho_T & 0 \\ \rho_p'\mathbf{Y} & \rho_{\mathbf{Y}}\mathbf{Y}+\rho & 0 & \rho_T\mathbf{Y}^T & 0 \\ \rho_p'\mathbf{V} & \rho_{\mathbf{Y}}\mathbf{V} & \rho\bar{\mathbf{I}} & \rho_T\mathbf{V}^T & 0 \\ \rho_p'h^0-(1-\rho h_p) & \rho_{\mathbf{Y}}h^0+\rho h_{\mathbf{Y}} & \rho\mathbf{V}^T & \rho_T h^0+\rho h_T & 0 \\ \rho_p'\mathbf{K} & \rho_{\mathbf{Y}}\mathbf{K} & 0 & \rho_T\mathbf{K} & \rho \end{pmatrix} \tag{4}$$

where the primed quantities refer to scaled values that control the accuracy and efficiency of the pseudo-time iterations.

B. Turbulence Model

The present simulations describe the large-scale, time-dependent turbulence motion by means of a Detached Eddy Simulation (DES) model. [14,15] DES is a hybrid RANS/LES approach which combines the RANS model in the attached boundary layers with the LES method in the large separation and wake regions.

A DES model can be obtained from any RANS model and our DES formulation uses the k-omega two-equation model with the appropriate modifications. Switching from RANS to LES mode is enabled by appropriately reducing the dissipation term in turbulent kinetic energy transport equations. Specifically, the DES model replaces the length scale with the minimum of the length scale defined in turbulence model for RANS and maximum spacing of the local grid as:

$$l_{DES} = \min\left(l_{k-\omega}, C_{DES}\delta\right) \tag{5}$$

where $\delta = \max\left(\Delta x, \Delta y, \Delta z\right)$ represents the maximum grid spacing in any direction and C_{DES} is a model constant and set equal to 0.78 as recommended by Travin et al.; $l_{k-\omega}$ is the length scale of Wilcox's k-w two equation model for the turbulence closure in RANS and it is defined as

$$l_{k-\omega} = \frac{k^{1/2}}{\beta^*\omega} \tag{6}$$

where β^* is a model constant. This definition of the length scale by Eq. (6) ensures that the RANS mode is utilized near the wall surface in which the high grid aspect ratio is typically expected. Finally, the dissipation term in the transport equation of the turbulence kinetic energy is replaced by

$$\beta^*\rho k w = \frac{\rho k^{3/2}}{l_{DES}} \tag{7}$$

This modification ensures that the resulting sub-grid model reduces to a Smagorinsky-like model at equilibrium.

C. Combustion Model

The six chemical species considered for the propellant combination in the LDI combustor are $C_{12}H_{23}$, O_2, CO_2, H_2O, CO and N_2. They are solved directly and turbulence transport in the species equations is modeled using the classical gradient model with a constant Schmidt number. Laminar finite rate chemistry model is used to evaluate the reaction rate. Although flamelets and transported-FMDF models are popular in unsteady LES simulations, their capabilities for predicting combustion/acoustic interaction problems are not well-established, particularly, because these models are based upon constant pressure flame assumptions.

We consider the fuel as $C_{12}H_{23}$ to approximate the experimental Jet-A fuel. A simplified two-step, five species global reduced mechanism has been incorporated in the present study. [16]

$$2\mathbf{C_{12}H_{23}} + 35\mathbf{O_2} \longrightarrow 24\mathbf{CO} + 23\mathbf{H_2O}$$

$$\text{and} \quad 2\mathbf{CO} + \mathbf{O_2} \longleftrightarrow 2\mathbf{CO_2}$$

The kinetics of the two-step global reactions are represented by an Arrhenius function of the form as:

$$\dot{\omega} = AT^n\left(-E_a / R_u T\right)\left[\mathbf{X_A}\right]^a\left[\mathbf{X_B}\right]^b \tag{8}$$

where w is the production rate, A is the pre-exponential constant, E_a is the activation energy, and n, a and b are exponents, respectively. For the first $C_{12}H_{23}$ oxidation step, the production rate is expressed with constants as

$2.643\times10^{9}\exp(-1.5108\times10^{4}/T)[C_{12}H_{23}]^{0.25}[O_2]^{1.5}$ (kmol/m^3-s). For the forward CO oxidization reaction in the expressed as $2.2387\times10^{12}\exp(-2.0143\times10^{4}/T)[CO][O_2]^{0.25}[H_2O]^{0.5}$ (kmol/m^3-s). It is expressed as $5.0\times10^{8}\exp(-2.0143\times10^{4}/T)[CO_2]$ (kmol/m^3-s) for the reverse CO dissociation reaction.

D. Fuel Spray Model

Comprehensive modeling of direct injection sprays for gas turbine engines has been developed for combustion dynamics problems. This method combines sub-models for atomizing, vaporizing and reacting sprays. Key physical events considered in the present model include free-surface jet in the atomizer, primary and secondary breakup, droplet vaporization, mixing and burning. The models are implemented within an Lagrangian-Eulerian framework, where the droplet phase is described by Lagrangian dynamics and the vaporized fuel is input as a source term along with associated momentum and energy terms in the Eulerian gas-phase equations.

There are three major submodels for the description of spray atomization: atomizer free surface flow, primary and secondary atomization models. The first submodel is the atomizer free surface flow. Independent calculation of the free surface internal flow in the atomizer is used to provide the spray injection conditions of the Lagrangian spray particles. Ashraf and Jog's numerical model [17] is employed for the present study. This model directly solves the two phase flow using the Eulerian Volume-Of-Fluid Method and provides the spray angle, liquid sheet thickness and velocity. This information is delivered to the primary atomization model, which is the second submodel. The primary atomization is described by the linear stability analysis of the liquid sheet proposed by Senecal et al. [18] Using the liquid sheet thickness and velocity, the most unstable wave length and maximum growth rate are determined by dispersion relation derived from linear stability theory, and ligament and drop sizes disintegrated from the liquid sheet are then calculated. Lagrangian drops produced by the primary atomization are defined at the exit plane of the atomizer and then undergo the secondary atomization process, which is in turn represented by the third sub-model. For the secondary atomization process, the drops may be broken up by several kinds of modes. The secondary atomization model developed in the present study covers the full Weber number range typically encountered in gas turbine combustors. Depending on the Weber number range, appropriate secondary atomization models are applied that include the Taylor Analogy Breakup (TAB), [19] Kelvin Helmholtz (KH) and Rayleigh-Taylor (RT) models.[20-22]

E. Dynamic Mode Decomposition (DMD) for Combustion Dynamics Diagnostics

Dynamic mode decomposition is a useful technique to examine modal information in the flowfield. The goal is to approximate a function, $z(x,t)$, over a domain of interest as a finite sum in the variables-separated form

$$z(x,t) \approx \sum_{k=1}^{M} a_k(t)\Phi_k(x) \tag{9}$$

with the reasonable expectation that the approximation becomes exact as M approaches infinity. Note that in Eq. (9) there is no fundamental difference between x and t, but we usually think of x as a spatial coordinate and t as the temporal coordinate.

The representation of Eq. (9) is not unique. For example, if the domain (experimental or computational) is a bounded interval X on the real line, then the functions $\Phi_k(x)$ can be chosen as a Fourier series, Legendre polynomials, Chebyshev polynomials, and so on. For different selections of the space-dependent function, $\Phi_k(x)$, the corresponding time-dependent function, $a_k(t)$, will be different. They can be periodic or non-periodic, single-frequency dominated or multi-frequency dominated.

In the case of the DMD analysis, in order to obtain single frequency dynamic modes, linear mapping is assumed from one snapshot to another. Detailed mathematical derivations can be found in Ref 23 and 24. Here the mathematics is briefly covered. Suppose the data set is represented as a snapshot sequence,

$$V_1^N = \{v_1, v_2, v_3, ..., v_N\} \tag{10}$$

where v_i stands for the i^{th} flowfield and $v_{i+1} = Bv_i$. The matrix B here represents the linear mapping matrix. Therefore,

$$V_1^N = \{v_1, Bv_1, B^2v_1, ..., B^{N-1}v_1\} \tag{11}$$

Another assumption is that there exists a specific number N, beyond which the vector v_N can be expressed as linear combination of the previous vectors,

$$v_N = a_1v_1 + a_2v_2 + ... + a_{N-1}v_{N-1} \quad \text{or} \quad v_1 = V_1^{N-1}a + r \tag{12}$$

Hence,

$$BV_1^{N-1} = V_2^N = V_1^{N-1}S + re_{N-1}^T \tag{13}$$

where,

$$S = \begin{pmatrix} 0 & & & & a_1 \\ 1 & 0 & & & a_2 \\ & \ddots & \ddots & & \vdots \\ & & 1 & 0 & a_{N-2} \\ & & & 1 & a_{N-1} \end{pmatrix} \tag{14}$$

Applying the eigenvalue decomposition for matrix *S*,

$$S = T^{-1}\Lambda T \tag{15}$$

where matrix *T* is the eigenvector matrix of *S*. If a sufficient number of snapshots are used, the eigenvalues of *S* are representative of the eigenvalues of *A*, which contains the time-evolution information of the flowfield.

Similarly the dynamic modes corresponding to single frequency response can be constructed as,

$$\Psi = V_1^{N-1}T^{-1} \tag{16}$$

The original data set can be decomposed into the form in Eq. (9),

$$V_1^{N-1} = \Psi T \tag{17}$$

where matrix Ψ contains the dynamic spatial information and matrix *T* contains the temporal evolutional information.

F. Computational Geometry and Operating Conditions

The geometries of the single LDI element used in the simulation are shown in Fig. 1. The reduced geometry, in Fig. 1 (a), was used to perform detailed studies of couplings between hydrodynamics and combustion, which have already been found to be important for combustion instabilities in a single LDI element configuration. [6] The reduced geometry uses an acoustically-open inlet and outlet to reduce or eliminate acoustic coupling with the hydrodynamics and combustion response. Otherwise, the reduced geometry used the same configuration of the fuel injector and swirler as the full geometry.

The full geometry in Fig. 1 (b) is the same as the one that was used in the experiments. In Fig. 1 (b), choked inlet slots (Detail A) and an exit nozzle (Detail C) are used to guarantee acoustically reflecting boundary conditions to sustain combustion instabilities in both the simulations and the experiments. Fuel injector (Detail B) sits in the converging-diverging section connecting the air plenum and combustor with the swirler. Preheated air comes through the choked inlet slots and enters the converging-diverging section through the air plenum. Hot air mixes with fuel spray from the fuel injector near the swirler and reacts in the combustor. The length of the air plenum and combustor are adjusted so that it supports a 3/8 acoustic wave in the air plenum and 1/2 wave in the combustor. Operating conditions vary in the inlet air temperature (T_{air}) and equivalence ratio (Φ). The location of the fuel injector was also changed to further investigate geometry effects. Table 1 summarizes the full geometry simulation cases used in this paper. Specifically, we consider two equivalence ratios (0.42 and 0.6) and two fuel injector locations, viz. at the venture throat (FT) and upstream of the throat (FU).

III. Results

In the Results section, DMD analysis of non-reacting flow simulation in the reduced geometry (fuel injector upstream) is given in Part A. The purpose of these initial studies is to identify important hydrodynamic modes that exist in the LDI combustor. The fuel spray modeling effects are summarized in Part B to provide a comparison of model performance for a representative case. Comparisons of the pressure oscillations between experiments and simulations are given in Part C for the cases listed in Table 1. In Part D, detailed cycle studies are carried out for the cases with the fuel injector located upstream (FU), with corresponding DMD results provided in Part E.

(a) Reduced geometry

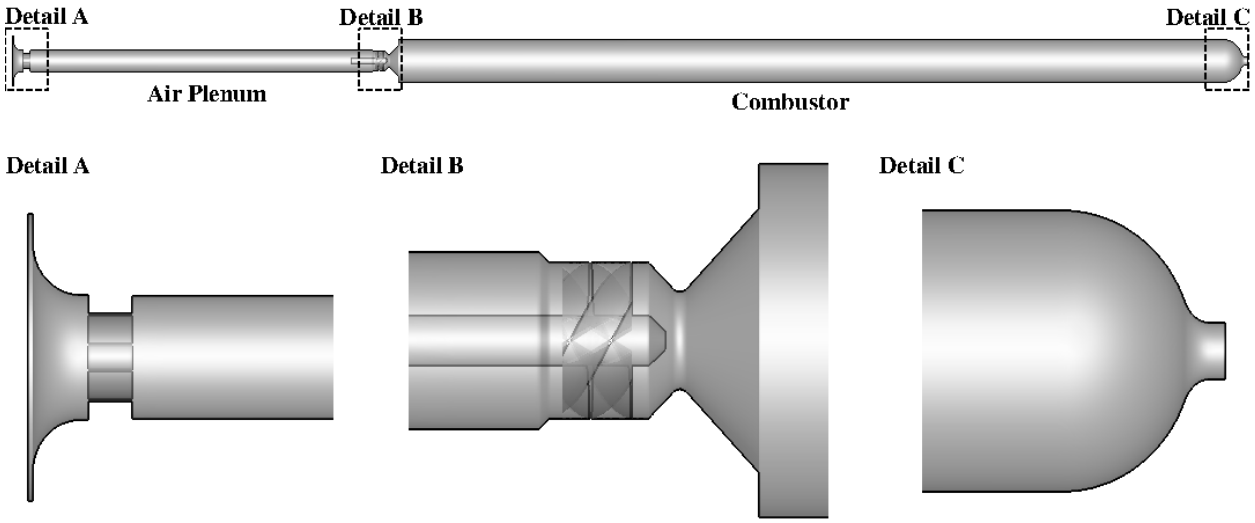

(b) Full geometry

Figure 1. Computational geometry of LDI gas turbine combustor.

T_{air}, K	Fuel Injector Location	Case Name	Φ
800	At throat of converging-diverging venturi	FT-1	0.42
		FT-2	0.6
	2.66mm upstream to the throat of converging-diverging venturi	FU-1	0.42
		FU-2	0.6

Table 1. Summary of simulation cases with full geometry

A. Non-reacting flow simulation with reduced geometry with T_{air} = 800K

Non-reacting flow simulation using the reduced geometry was performed to investigate the hydrodynamics alone without the influence of acoustics and combustion. In addition, in order to eliminate any uncertainties arising from the fuel spray model, no fuel was introduced in this reduced-geometry simulation. The same air mass flow rate and air temperature (800K) as in the full geometry simulations were used with 1MPa specified as the back pressure at the exit plane in Fig. 1 (a).

DMD analysis was applied to investigate important dynamic modes introduced by the LDI-element flow field. The DMD spectrum is shown in Fig. 2. Identifiable harmonic modes can be categorized based on the frequencies. The PVC modes are dominant in the high frequency region (> 4,000Hz) while in the low frequency region (< 3,000Hz), the so-called spinning modes are dominant. Those two sets of modes are important hydrodynamics phenomena introduced by the swirling flow and the converging-diverging venturi. In previous reduced geometry non-reacting simulations with the fuel injector located at the venturi throat, the fundamental PVC frequency was

reported to be around 3,000 and air temperature was kept at 700K. [6] The nature of PVC instability has been identified and described by Syred et al. [25,26]

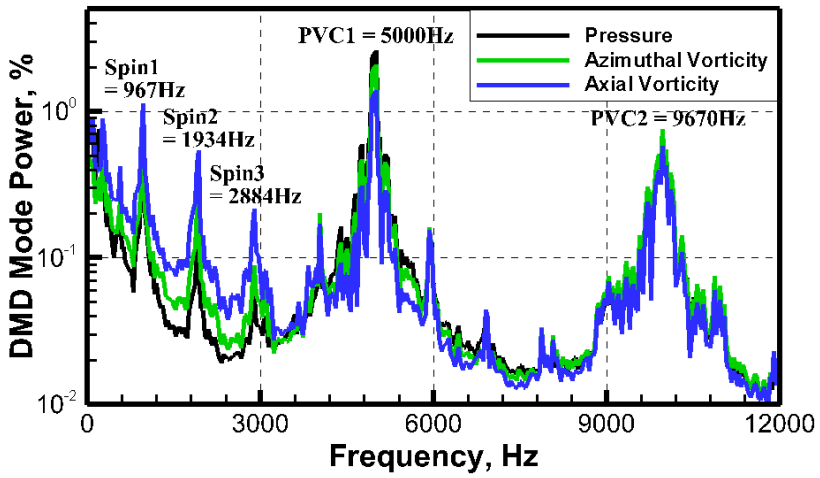

Figure 2. DMD spectrum of reduced geometry simulation with T_{air} = 800K (no fuel spray).

Representative responses of the PVC and spinning modes obtained from the DMD analysis are shown in Fig. 3 and Fig. 4 respectively for the pressure, axial and azimuthal vorticity variables. The PVC modes clearly indicate the presence of strong vortical structures in all of the three variables selected. Moreover, dynamic responses of the PVC modes are restricted to the diverging section of the venturi, which can be a strong potential driving force for fuel/oxidizer mixing in the combustor head region.

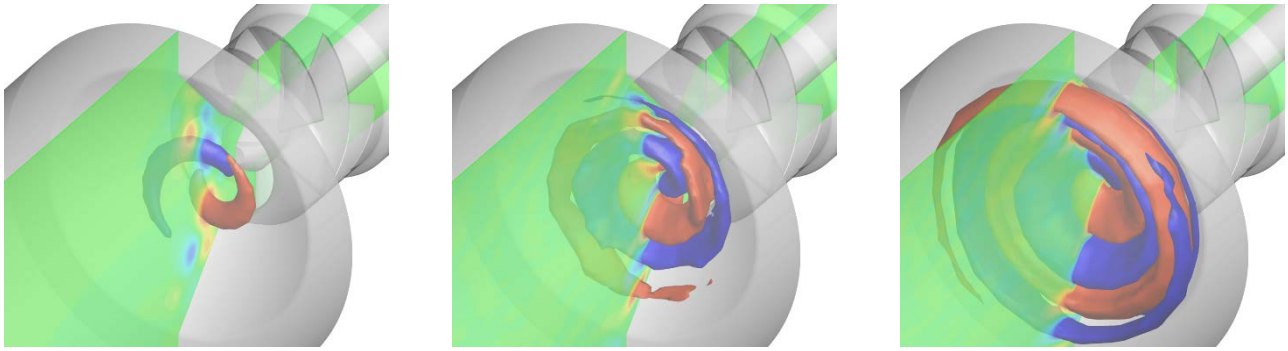

Pressure Axial Vorticity Azimuthal Vorticity

Figure 3. Dynamic modes at 1st PVC mode frequency from DMD analysis.

Distinct from the PVC modes, the spinning modes lie in a low frequency region, which are in fact quite close to the longitudinal acoustic modes observed in the full geometry simulations (shown later). Dynamic responses of the spinning modes are more stretched and extend downstream to the diverging section of the venturi, which can further make it easier for these modes to interact with the longitudinal acoustics especially at the lower frequencies (e.g. 1L, 2L, 3L, 4L etc).

Detailed studies are required to determine how these hydrodynamic modes interact with the acoustic modes and the spray and combustion responses and how they can be drive or damp combustion instabilities in the LDI configuration. Such studies are discussed in the following sections, but first we attempt to characterize the fuel spray model used in this work.

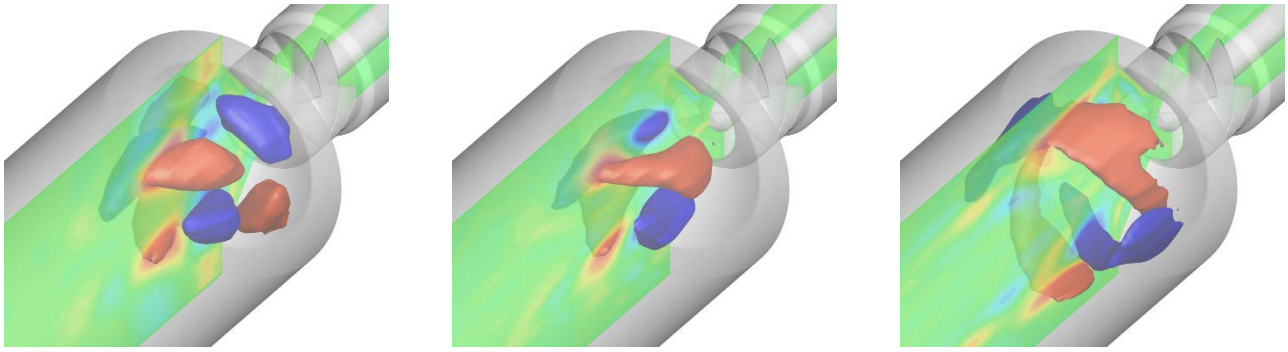

Pressure Axial Vorticity Azimuthal Vorticity

Figure 4. Dynamic modes at 1st Spinning mode frequency from DMD analysis.

B. Overview of Fuel Spray Modeling Effects

Fuel spray modeling is a key factor in the high-fidelity predictions of combustion instability in the LDI combustor. To date, four types of fuel spray models have been applied in our work. The four spray models and their effects on the predictions of the pressure amplitudes and the dominant acoustic mode are summarized in Table 2 for the equivalence ratio of 0.60. Comparisons of the first three models (Case 1 to 3) have been reported previously in Ref 6, while the fourth model corresponds to the present research. It should be noted that the comparisons are based on slightly different inlet air temperatures. The experiments and the present computations employ an air temperature of 800K, while the previous three computations are for a temperature of 750K. It has been reported that in high temperature regime (T_{air} > 750K), temperature variations do not influence the fuel spray performance much[27] so the comparisons given here may be justifiable. We note that the four spray models represent a progressive improvement in the sophistication of the fuel spray model and the results also reflect this trend, albeit not perfectly. The simplest model, which is the log-normal droplet distribution model, is capable of predicting self-excited combustion instability in the LDI element,[3] but it over-predicted the pressure amplitude and the wrong dominant acoustic mode. The second model or the single drop injection model predicted similar pressure amplitudes as the experiment but the dominant acoustic mode again did not match experiment. The hollow cone injection model was able to predict the correct dominant acoustic mode (4L) but the pressure amplitude was significantly under-predicted. Finally, the current hybrid model provided reasonable prediction of the dominant acoustic mode (3L vs. 4L), but still strongly under-predicts the pressure amplitude compared to the experiments. We further note that no attempts have been made at this stage to calibrate the models. Better understanding of parametric performance is needed before such calibrations are carried out.

Operating Conditions	Case Name	Total peak-to-peak pressure amplitude (%)	Dominant Acoustic Mode	Secondary Atomization Model
T_{air} = 800K, Φ = 0.6	Experiment	8	4L	-
T_{air} = 750K, Φ = 0.6	Case 1: Log Normal Distributed Drop Injection	11	1L	No
	Case 2: Single Drop Injection	7	2L	KH
	Case 3: Hollow Cone Injection	0.24	4L	KH
T_{air} = 800K, Φ = 0.6	Case 4: Hybrid Model	0.7	3L	Hybrid TAB/KH/RT

Table 2. Summary of fuel spray modeling effects on predicting combustion instability.

The associated heat release and drop distributions are visualized in Fig. 5 using instantaneous snapshots of the simulation results. Cases 1, 2 and 4 indicate complete fuel spray breakup before entering the combustor head and the drops are restricted to the diverging section while Case 3 shows more penetration and longer lasting fuel spray

distribution downstream. As reported in Ref 6, the KH model is not capable of describing the secondary atomization under the conditions prevalent in Case 3, which explains why more drops remain downstream of the injector element. This was, in fact, the major motivation to develop the present hybrid model. The heat release distributions show that there is a strong combustion response in the diverging section of the venturi for all four cases. But, the combustion distribution in the combustor beyond the diverging section varies for the different fuel spray models. Case 1 predicts the most concentrated reaction zone and combustion occurs even in the central region, which was not observed in the other three cases. Case 2 indicates more stretched heat release distribution than Case 1, while the flame seems to be detached from the combustor wall compared with Cases 3 and 4 where it seems to follow the flow separation near the walls. It is interesting to note that Cases 3 and 4 predict very similar heat release distributions, which are more stretched than in the other two cases.

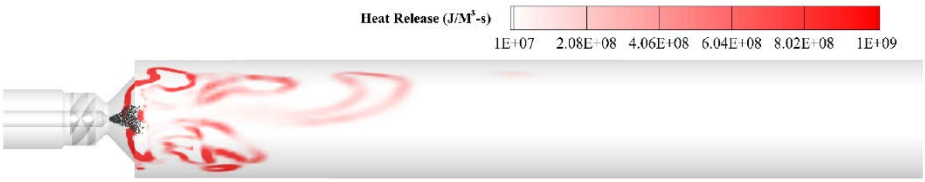

(a) Case 1: Log Normal Distributed Drop Injection

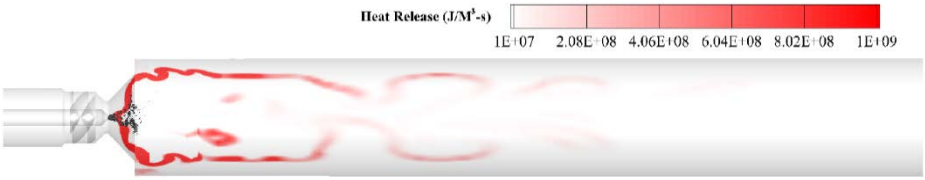

(b) Case 2: Single Drop Injection

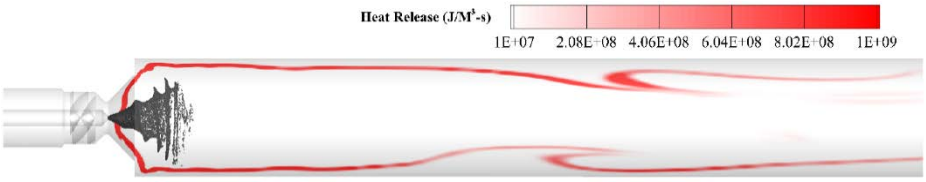

(c) Case 3: Hollow Cone Injection

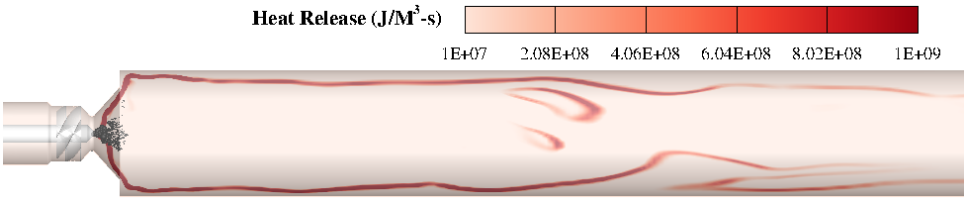

(d) Case 4: Hybrid Model

Figure 5. Instantaneous heat release contours in terms of different fuel spray modeling.

C. Pressure Signal Comparisons with Experiment

Comparisons between the computed and measured pressure signals are discussed in this section for two operating conditions and two fuel injector locations. Comparisons with the fuel injector at the throat (FT) are shown in Figs. 6 and 7 under high (FT-1, Φ = 0.6) and low (FT-2, Φ = 0.42) equivalence ratios respectively. In both experiments and simulations, the pressure amplitude is higher for the higher equivalence ratio. However, the simulations under-predict the pressure amplitudes. The PSDs of pressure from simulation is off by 2 orders of magnitude compared with the experimental PSD's. In the high equivalence case, dominant peaks can be found at 1L, 3L and 7L in the simulated results, while the experiments indicate 4L, 8L and peaks at around 7,000Hz. In the

low equivalence ratio case, the simulations predict more evenly distributed PSD of pressure oscillations while experiment still shows same dominant peaks as in the high equivalence ratio case.

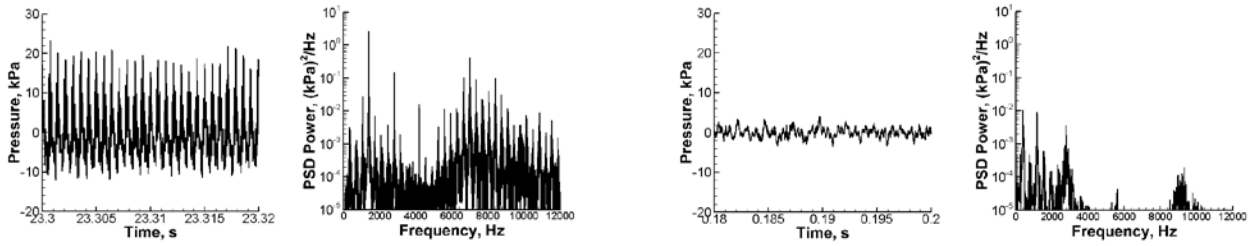

Experiment Simulation

Figure 6. Case FT-1 comparisons between simulation and experiment in high-pass filtered pressure signal and its PSD with pressure measured at the same location at combustor head section.

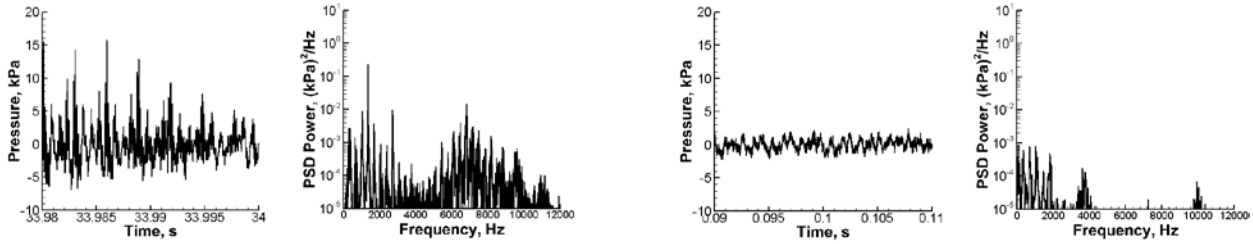

Experiment Simulation

Figure 7. Case FT-2 comparisons between simulation and experiment in high-pass filtered pressure signal and its PSD with pressure measured at the same location at combustor head section.

Comparisons with fuel injector upstream to the throat (FU) are shown in Figs. 8 and 9 for the high (FU-1, Φ = 0.6) and low (FU-2, Φ = 0.42) equivalence ratios respectively. Good agreement is observed for the FU-1 case with regard to the pressure amplitudes (~100kPa peak-to-peak amplitude, which corresponds to ~10% combustion instability level relative to the 1MPa mean chamber pressure). The 4L acoustic mode is observed to be dominant in the simulations by looking at both the pressure signal and PSD plot. Acoustics in the combustor shows well-defined harmonic behavior at multiples of the 4L frequency, while the other longitudinal acoustic modes (e.g. 1L, 2L and 3L) are not as strong. In the experiments, dominant peaks stand out at 4L, 8L and in the frequency range between 7,000 and 8,000Hz (where the magnitudes are comparable to the 8L amplitude). The simulations match reasonably well with the experiment in predicting the dominant acoustic modes. However, it is noted that experiment shows higher PSD power in the other acoustic frequencies which are not significant in the simulations. In addition, the simulations do not fully capture the high frequency mode in between 7,000 and 8,000Hz.

For FU-2 case, both simulation and experiment show lower pressure oscillation amplitudes (~6% combustion instability level) compared with FU-1 case. Though the amplitudes reach agreement to some extent, there is a discrepancy in predicting the dominant acoustic modes. In the simulations, the high frequency mode (~7,000Hz) is not present. Importantly, the simulations predict dominant frequencies at 4L and 5L, while the experimental data shows more evenly distributed energies for each acoustic mode with the 1L mode being the strongest. More detailed validation work needs to be done to figure out the origin of the discrepancy between simulations and experiments. The major uncertainty still appears to be the fuel spray model, which was addressed in Part B. As noted earlier, the present computations are not calibrated in any way.

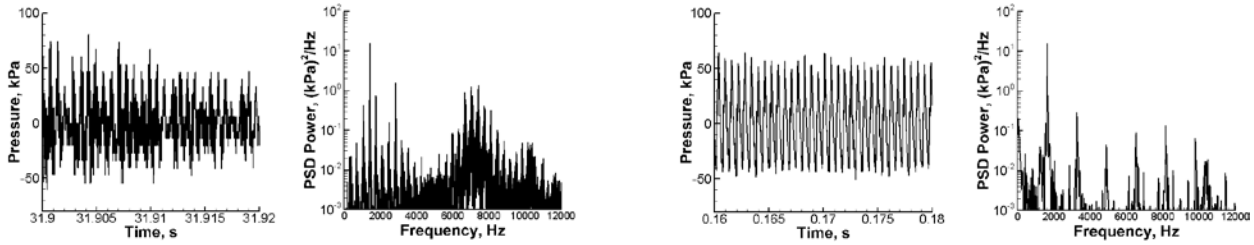

Experiment Simulation

Figure 8. Case FU-1 comparisons between simulation and experiment in high-pass filtered pressure signal and its PSD with pressure measured at the same location at combustor head section.

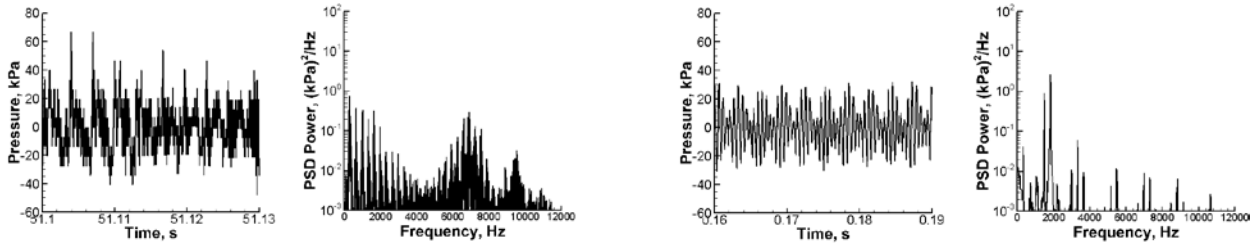

Experiment Simulation

Figure 9. Case FU-2 comparisons between simulation and experiment in high-pass filtered pressure signal and its PSD with pressure measured at the same location at combustor head section.

D. Cycle studies of full geometry simulations

Detailed studies based on the cyclic behavior and interactions between flame, flow and acoustics in the combustor are performed for the two FU simulation cases since they indicate better agreement with the experimental measurements than the FT cases. A single cycle based on the dominant frequencies in the PSD plots in Figs. 8 and 9 has been selected.

(1) FU-1 (T_{air} = 800K, Φ = 0.6)

Six representative cycle snapshots are shown in Fig. 10 to illustrate the thermo-acoustical interactions under this operating condition. As discussed in Part C, the 4L acoustic mode was found to be dominant in both the simulations and experiments; the cycle period (T_{cycle}) was therefore determined based on the 4L frequency and the 4L mode can be clearly observed in the pressure contours. t_0 represents the start of the cycle and each snapshot represents an increment of $1/6T_{cycle}$ in time. Starting at t_0, the pressure reaches its peak at the combustor head and travels downstream towards the exit nozzle (snapshot (a)). It reaches its minimum at the combustor head in snapshot (c). Snapshot (a) to (c) can be thought of as an expansion process at combustor head end, during which both the fuel mass fraction and azimuthal vorticity are decreasing. This in turn leads to a decrease in the heat release level since less fuel is being fed into the reaction and the decreasing azimuthal vorticity results in less mixing between fuel and oxidizer. Thus, the heat release decreases with pressure in this process. After snapshot (c), the pressure wave starts to return back to head-end. So, snapshot (d) to (f) can be thought of as a compression process at the combustor head. During this latter half of the cycle, vortices rotating in the azimuthal direction start to be accelerated by the returning pressure wave, which in turn increases the level of azimuthal vorticity and helps enhance the mixing between the gaseous fuel and air. Moreover, the level of fuel mass fraction also increases and therefore heat release level increases correspondingly. Thus, during the acoustic compression process, heat release increases in phase with the pressure increase. It can therefore be concluded that the heat release varies in phase with the pressure oscillations and according to Rayleigh criterion, [28] this means that combustion instability is being driven in the combustor.

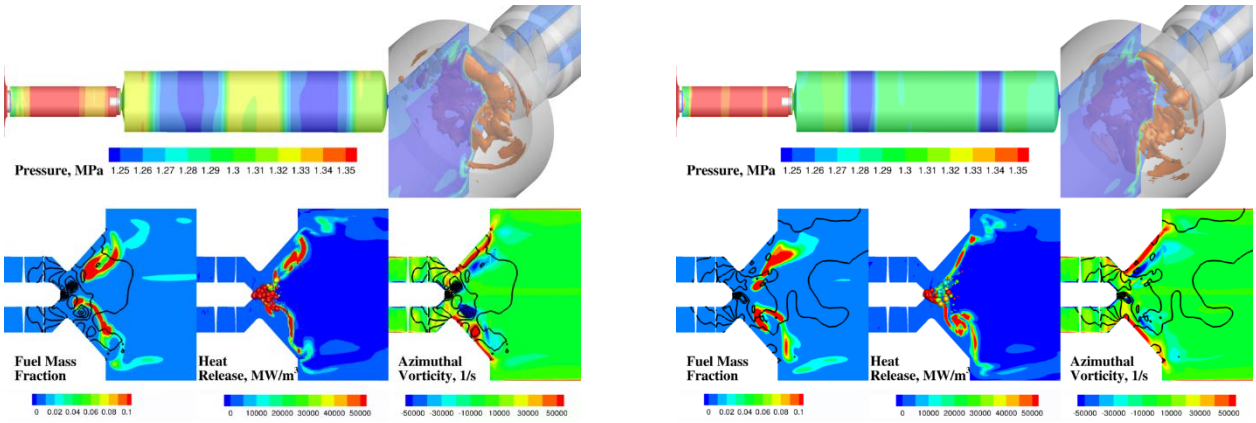

(a) $t=t_0$ (b) $t=t_0 + 1/6\ T_{cycle}$

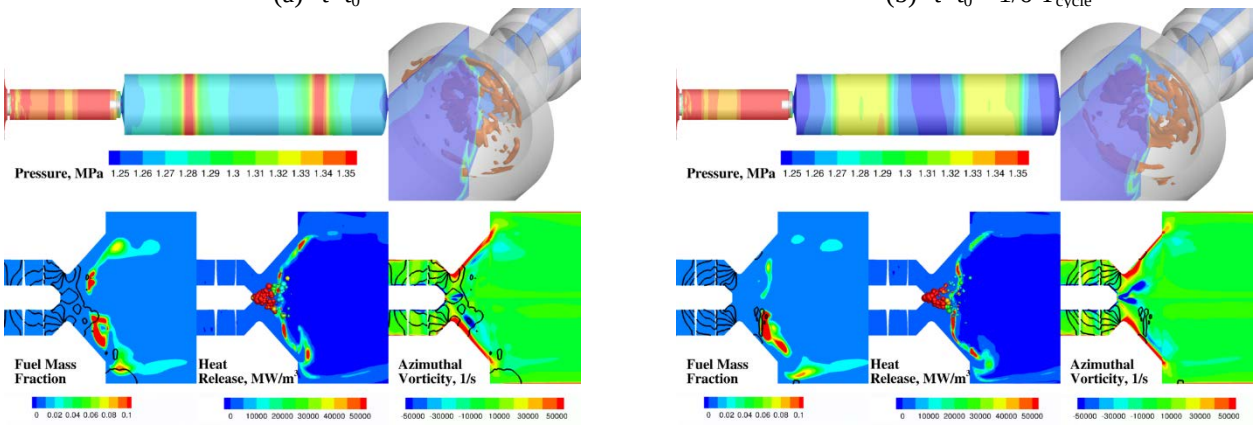

(c) $t=t_0 + 2/6\ T_{cycle}$ (d) $t=t_0 + 3/6\ T_{cycle}$

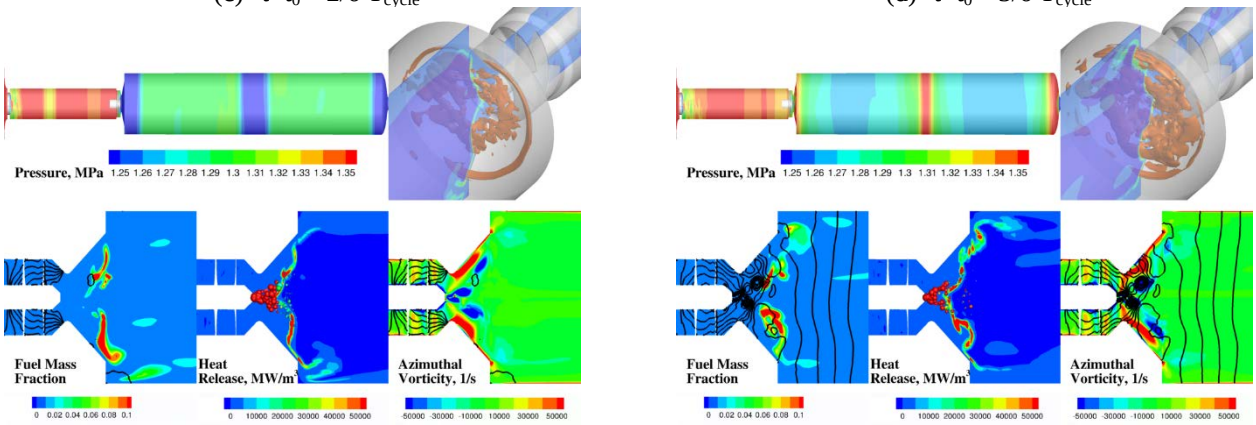

(e) $t=t_0 + 4/6\ T_{cycle}$ (f) $t=t_0 + 5/6\ T_{cycle}$

Figure 10. Cycle snapshots for FU-1 case. First row: left, pressure contour at center slice; right, heat release iso-surface at 50,000 MW/m^3 with its contour at center slice. Second row: left, fuel mass fraction contour at center slice with contour line of pressure; middle, heat release contour at center slice with spray colored by Weber number; right, azimuthal vorticity contour at center slice (+: counterclockwise; -: clockwise) with contour line of pressure.

(2) FU-2 (T_{air} = 800K, Φ = 0.42)

The snapshots for the lower equivalence ratio simulation in Fig. 11 are shown in the same way as those for the higher equivalence ratio case. Based on the PSD plots of pressure, the 4L and 5L are the two dominant acoustic modes and, similarly from the pressure contours, 4L and 5L modes show up alternatively and the cycle period is still picked based on 4L frequency. Again, we can define the expansion (snapshots (a) to (c)) and compression (snapshots (d) to (f)) processes at the combustor head. However, the physics observed here is different from that for the high equivalence ratio case. First, more spray drops are present in the diverging section and, while the fuel mass fraction still decreases during expansion and increases during compression, the variation level is conspicuously lower. One possible reason is that, in both simulation and experiment, the equivalence ratio is changed by varying the fuel mass flow rate while keeping the air mass flow rate fixed. By lowering the fuel spray mass flow rate, the spray velocity decreases so that the drops are less susceptible to break-up, which brings down the variations of the fuel mass fraction. Secondly, the azimuthal vorticity stays stationary and relatively constant compared to the FU-1 case. This is because, in the low equivalence ratio case, the pressure oscillation level is lower, which indicates less acoustic driving of the flow-field and therefore the hydrodynamics stays relatively stable. Thus, the less tight coupling between the heat release and pressure oscillations in the FU-2 case leads to lower combustion instability levels. It would be expected that, with even lower equivalence ratio, the level of instability would be suppressed more and will eventually result in stable behavior.

E. Dynamic Mode Decomposition Analysis

Modal analysis was applied to investigate the important dynamics at the dominant frequencies of interest for the full geometry simulations with the fuel injector located upstream of the throat. The DMD spectrum is shown in Fig. 12. In the FU-1 case (Fig. 12 (a)), the acoustics follows a well-defined harmonic behavior at the 4L frequency. The combustion response (represented by heat release) and hydrodynamic response (represented by azimuthal vorticity) follow the acoustic response at the 4L and 8L frequencies while some high frequency dynamics (e.g. 3,736 Hz and 5,370 Hz) are also present in the heat release and azimuthal vorticity spectrum. In the FU-2 case (Fig. 12 (b)), the 4L and 5L are the two dominant acoustic modes based on the DMD pressure spectrum. Similar to the FU-1 case, heat release and azimuthal vorticity both have responses driven by longitudinal acoustics as well as a high energy peak in the high frequency region (at 6504 Hz).

Representative instantaneous dynamic responses have been extracted at specific frequencies for the two FU cases and are shown in Fig. 13. At the dominant longitudinal frequencies (4L for the FU-1 case and 5L for the FU-2 case), corresponding acoustic mode shapes can be observed in the combustor. The heat release shows a well-defined ring structure in the three-dimensional iso-surface view. The instantaneous snapshots have been selected when the pressure is high at the combustor head for both cases. It is noted that, when the pressure is high, the fuel mass fraction and azimuthal vorticity are also at a high level so that the heat release increases in phase with the pressure. However, the variation level of the fuel mass fraction and azimuthal vorticity is lower in the FU-2 case, which brings the heat release oscillations down consequently so that the pressure amplitude is lower for this case.

Looking at the responses at high frequencies (5,370Hz for the FU-1 case and 6,504Hz for the FU-2 case), the acoustic responses in the combustor are weaker than those at the longitudinal acoustic frequencies. The main acoustic responses are restricted within the diverging section, visualized by the pressure contour lines. Unlike the ring structure mentioned above, the heat release responses at high frequencies clearly indicate three-dimensional vortical structures that can be largely driven by the swirling flow at the combustor inlet. The vortical structures observed here are also consistent with the ones that are found in non-reacting simulation in the reduced geometry (Fig. 3). This confirms the influence of the PVC hydrodynamic mode on the combustion dynamics in the LDI combustor configuration.

The reacting results, however, do not show specific evidence of the spinning mode, observed in Fig. 4, but it is likely that the spinning mode interacts with the longitudinal acoustic mode directly, which can help explain why the higher acoustic modes (4L and 5L) are being driven rather than the 1L as seen in our rocket combustor studies.[29]

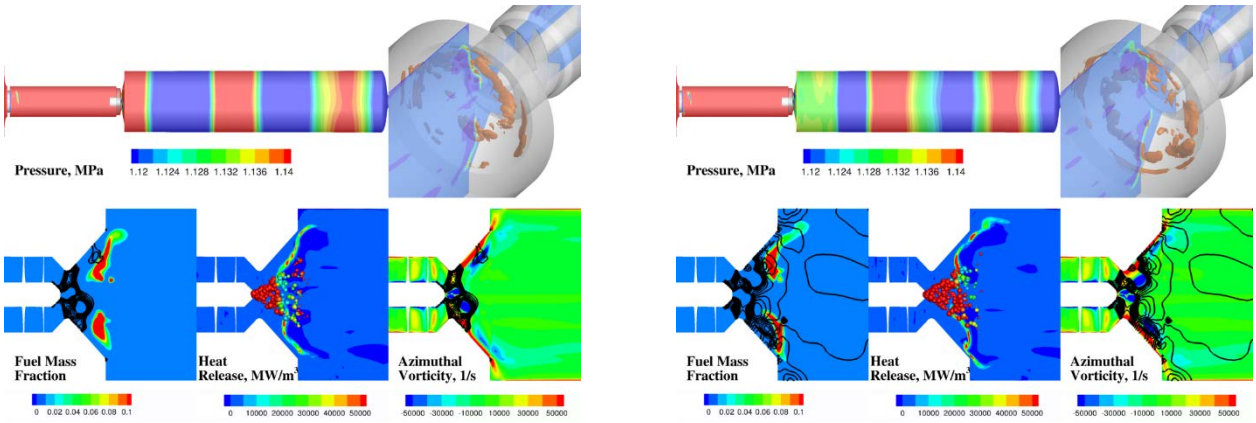

(a) $t = t_0$ (b) $t = t_0 + 1/6\ T_{cycle}$

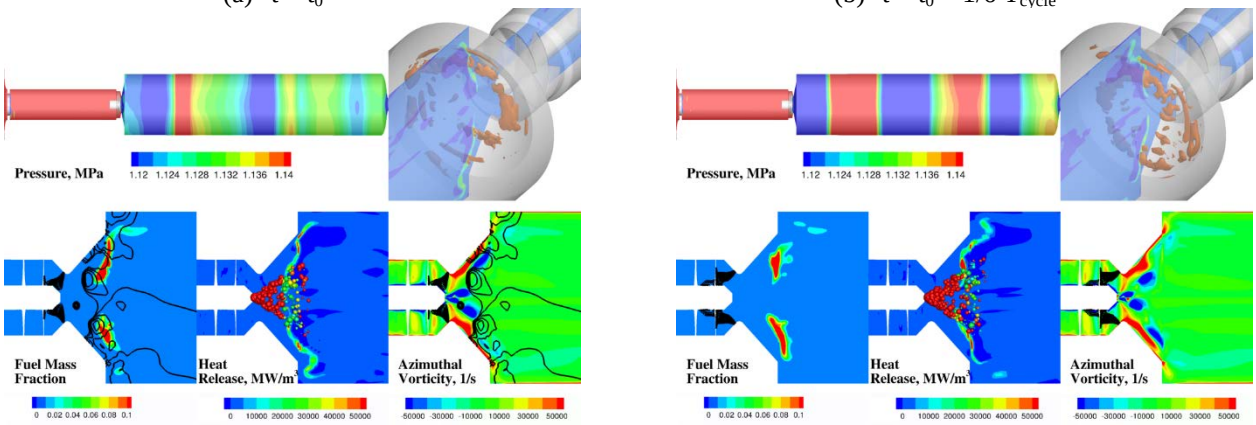

(c) $t = t_0 + 2/6\ T_{cycle}$ (d) $t = t_0 + 3/6\ T_{cycle}$

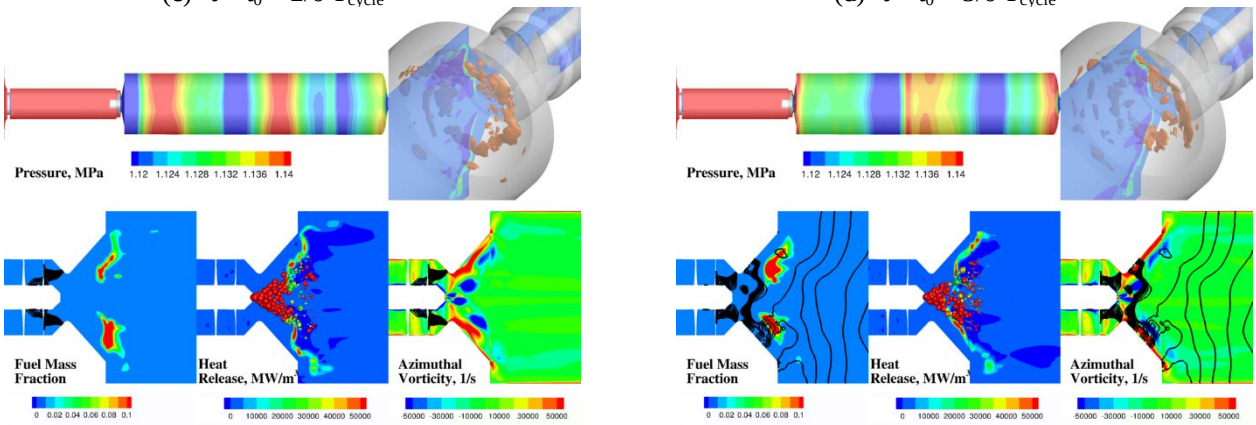

(e) $t = t_0 + 4/6\ T_{cycle}$ (f) $t = t_0 + 5/6\ T_{cycle}$

Figure 11. Cycle snapshots for FU-2 case. First row: left, pressure contour at center slice; right, heat release iso-surface at 50,000 MW/m^3 with its contour at center slice. Second row: left, fuel mass fraction contour at center slice with contour line of pressure; middle, heat release contour at center slice with spray colored by Weber number; right, azimuthal vorticity contour at center slice (+: counterclockwise; -: clockwise) with contour line of pressure.

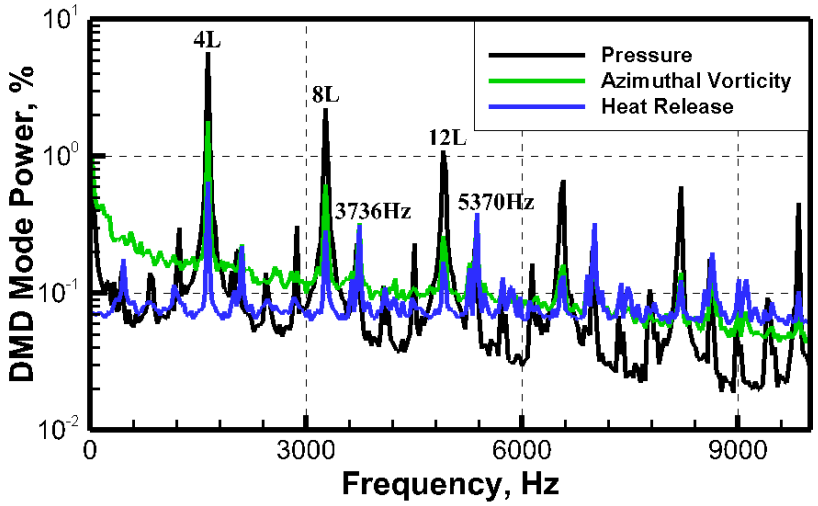

(a) FU-1 (T_{air} = 800K, Φ = 0.6)

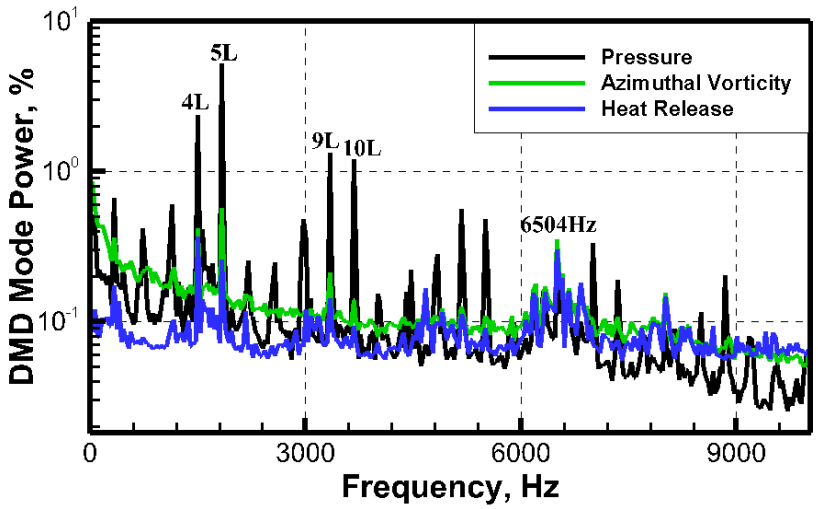

(b) FU-2 (T_{air} = 800K, Φ = 0.42)

Figure 12. DMD spectrum of full geometry simulations (FU cases).

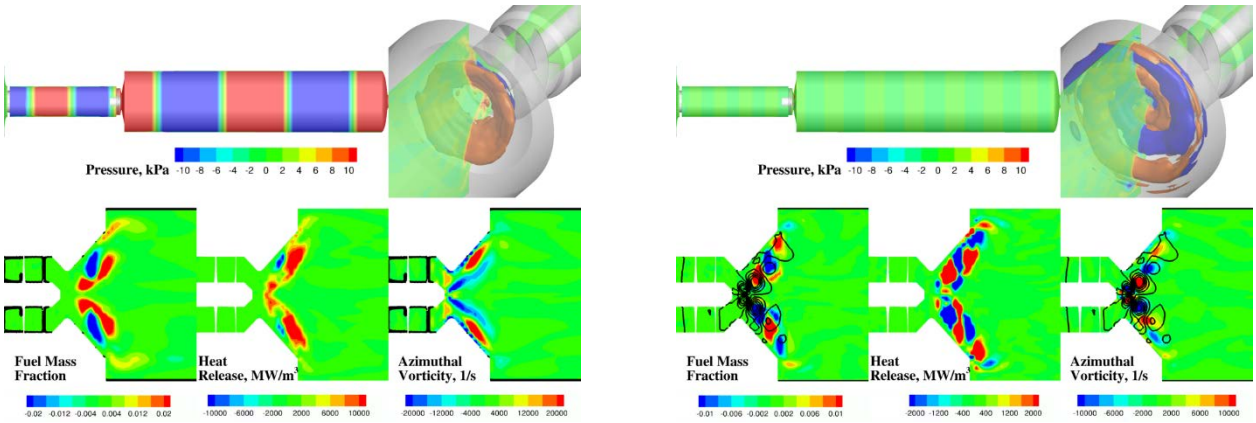

Dynamic responses at 4L frequency Dynamic responses at 5,370Hz

(a) FU-1 (T_{air} = 800K, Φ = 0.6)

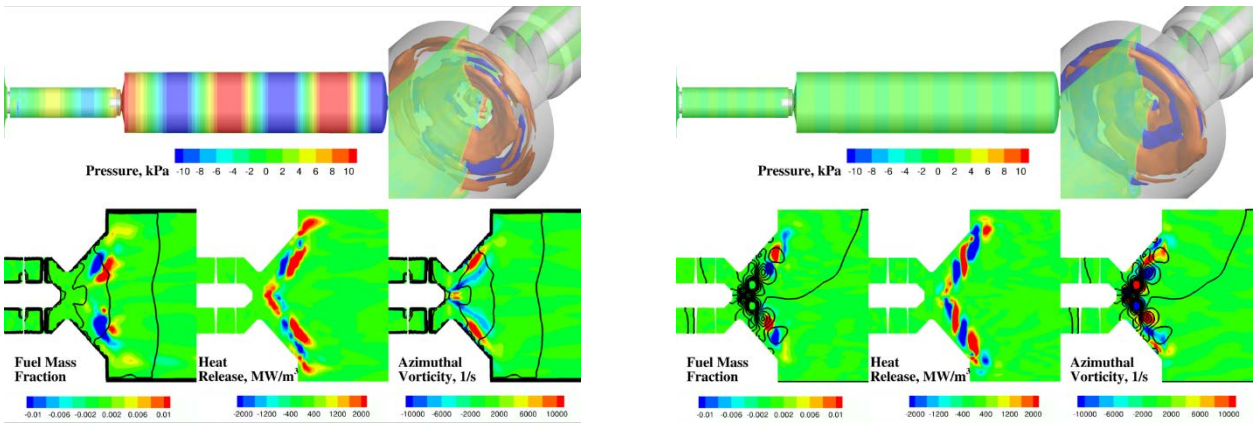

Dynamic responses at 5L frequency Dynamic responses at 6,504Hz

(b) FU-2 (T_{air} = 800K, Φ = 0.42)

Figure 13. Instantaneous DMD responses at specific frequencies from FU cases simulations. First row: left, pressure contour at center slice; right, heat release iso-surface at ±10,000 MW/m^3 with its contour at center slice. Second row: left, fuel mass fraction contour at center slice with contour line of pressure; middle, heat release contour at center slice with spray colored by Weber number; right, azimuthal vorticity contour at center slice (+: counterclockwise; -: clockwise) with contour line of pressure.

IV. Conclusions

Self-excited combustion instability was investigated computationally in a laboratory-scale single element LDI gas turbine combustor. Computations were performed with both a reduced and full geometry to study important modes from the acoustics, combustion and hydrodynamics. Analysis of the reduced geometry that did not include the exit nozzle, the fuel spray or combustion provides a clear understanding of the important hydrodynamic modes present in the LDI combustor. The precessing vortex core (PVC) mode has been observed, the responses of which are restricted to the diverging section of the venturi. In addition, another low frequency hydrodynamic mode , referred to as the spinning mode, has also been identified using DMD analysis. We further note that the frequencies of the spinning mode are in the range of the 4L and 5L acoustic modes for the full geometry with the nozzle.

Experimental data is available to compare the high-fidelity simulations using full geometry. Our current results utilize high inlet air temperature (T_{air} = 800K) with different fuel injector locations and equivalence ratios. Based on the comparisons of the pressure signal, simulations with the fuel injector at the throat under-predicted the level of combustion instability and the magnitude of the pressure PSD is nearly 2 orders of magnitude lower than the experiment. Simulations with the fuel injector upstream of the throat compares better with the experimental measurement but it does not fully capture the high frequency response around 7,000Hz. Simulations with the high

equivalence ratio match the experimental results well in predicting the dominant acoustic modes (4L, 8L). However, with the low equivalence ratio, some discrepancies remain with the simulations indicating dominant responses at 4L and 5L, while the experiments show more evenly distributed acoustic modes with 1L being dominant. As mentioned above, fuel spray modeling is probably the major uncertainty in the simulations and more effort will be put to calibrate the models to try to match experimental trends better.

Detailed cycle studies were performed for fuel injector upstream cases to illustrate the mechanisms that drive the combustion instabilities in the LDI combustor. In the high equivalence ratio case, when the timing of heat addition is coupled with the acoustic compression process, combustion instability is driven, which is in agreement with the Rayleigh criterion. On the other hand, for the low equivalence ratio case, less variation in the heat release is observed leading to lower levels of combustion instability.

Dynamic mode decomposition (DMD) analysis was applied to investigate the dynamic motions under the frequencies of interest for both the full and reduced geometry simulations. In the analysis of the full geometry cases, the combustion responses at the dominant longitudinal acoustic frequency coupled well with the acoustic responses, consistent with the cycle studies. Identifiable vortical structures can be found in the heat release and vorticity dynamics modes, which is consistent with the PVC modes found in the non-reacting reduced geometry simulation. In summary, it is clear that the current simulations provide useful qualitative insight into the mechanisms underlying combustion instability even if quantitative validation remains a challenge.

Acknowledgements

The authors acknowledge the support of the NASA Glenn Research Center and Program Manager Mr. Kevin Breisacher in sponsoring the subject work under NASA Research Announcement (NRA) grant number NNX11AI62A and financial support from John Zink Company. Also, we would like to give special thanks to Drs. Charles Merkle and Hukam Mongia who set the original direction of the study and Dr. Phil Lee of Woodward for providing the fuel nozzle used in the experiment.

References

[1] Yi, T. and Santavicca, D. A., "Forced Flame Response of Turbulent Liquid-Fueled Lean-Direct-Injection Combustion to Fuel Modulations," *Journal of Propulsion and Power*, Vol. 25, No. 6, 2009, pp. 1259—1271.

[2] Cohen et al., "Longitudinal Mode Aeroengine Combustion Instability: Model and Experiment," NASA TM-2000-210067, NASA Glenn Research Center, 2000.

[3] Yoon, C., Gejji, R., Anderson, W.E. and Sankaran, V., "*Computational Investigation of Combustion Dynamics in a Lean Direct Injection Gas Turbine Combustor*", 51st Aerospace Sciences Meeting including the New Horizons Forum and Aerospace Exposition, January 07-10, 2013, Grapevine (Dallas/Ft. Worth Region), Texas

[4] Reitz, R., "Modeling Atomization Processes in High-Pressure Vaporizing Sprays, *Atomisation and Spray Technology*, Vol. 3, 1987, pp. 309-337.

[5] M. Patterson and R. Reitz, Modeling the Effects of Fuel Spray Characteristics on Diesel Engine Combustion and Emission, SAE 980131, 1998

[6] Yoon, C., Gejji, R., Anderson, W.E. and Sankaran, V., "*Effects of Fuel Spray Modeling on the Combustion Dynamics of Lean Direct Injection Model Combustor*", ILASS-Americas 25th Annual Conference on Liquid Atomization and Spray Systems, Pittsburgh, PA, May 2013.

[7] Yoon, C., Huang, C., Gejji, R., Anderson, W.E. and Sankaran, V., "*Computational Investigation of Combustion Instabilities in a Laboratory-Scale LDI Gas Turbine Engine*", 49th AIAA/ASME/SAE/ASEE Joint Propulsion Conference, July 14-17, 2013, San Jose, CA

[8] Li, D., Xia, G., Sankaran, V., Merkle, C. L., "Computational Framework for Complex Fluids Applications," *3rd International Conference on Computational Fluid Dynamics*, Toronto, Canada, July 12-16, 2004.

[9] Xia, G., Sankaran, V., Li, D., and Merkle, C.L., "Modeling of Turbulent Mixing Layer Dynamics in Ultra-High Pressure Flows", *36th AIAA Fluid Dynamics Conference and Exhibit*, San Francisco, CA, June 05-08, 2006, AIAA 2006-3729.

[10] Lian, C., Xia, G. and Merkle, C. Solution-Limited Time Stepping to Enhance Reliability in CFD Applications. Journal of Computational Physics, Vol. 228, 2009, pp. 4836-4857.

[11] Lian, C., Xia, G. and Merkle, C. Impact of Source Terms on Reliability of CFD Algorithms. *The 19th AIAA Computational Fluid Dynamics*, San Antonio, TX, June 22-25, 2009.

[12] Smith, R., Xia, G., Anderson, W.A., and Merkle, C.L. (2010), "Computational Simulations of the Effect of Back-Step Height on Non-Premixed Combustion Instability", *AIAA Journal*, V. 48, No. 9, pp1857-1868, September, 2010.

[13] Smith, R., Ellis, M., Xia, G., Sankaran, V., Anderson, W. and Merkle, C.L., „Computational Investigation of Acoustics and Instabilities in a Longitudinal-Mode Rocket Combustor," *AIAA Journal*, Vol. 46, No. 11, November 2008, pp. 2659-2673.

[14] D. Basu, A. Hamed, K. Das, and Asme, "DES, hybrid RANS/LES and PANS models for unsteady separated turbulent flow simulations," *Proceedings of the ASME Fluids Engineering Division Summer Conference, Vol 2*, pp. 683-688, 2005.

[15] R. A. Baurle, C. J. Tam, J. R. Edwards, and H. A. Hassan, "Hybrid Simulation Approach for Cavity Flows: Blending, Algorithm, and Boundary Treatment Issues," *AIAA Journal*, vol. 41, pp. 1463-1480, 2003.

[16] C. K. Westbrook and F. L. Dryer, "Simplified Reaction-Mechanisms for the Oxidation of Hydrocarbon Fuels in Flames," *Combustion Science and Technology*, vol. 27, pp. 31-43, 1981.

[17] I. Ashraf and M. A. Jog, "Nonlinear breakup model for a liquid sheet emanating from a pressure-swirl atomizer," *Journal of Engineering for Gas Turbines and Power-Transactions of the Asme*, vol. 129, pp. 945-953, Oct 2007.

[18] P. K. Senecal, D. P. Schmidt, I. Nouar, C. J. Rutland, R. D. Reitz, and M. L. Corradini, "Modeling high-speed viscous liquid sheet atomization," vol. 25, pp. 1073-1097, 1999/11// 1999.

[19] P. J. O'Rourke and A. A. Amsden, "The Tab Method for Numerical Calculation of Spray Droplet Breakup," 1987.

[20] J. C. Beale and R. D. Reitz, "Modeling spray atomization with the Kelvin-Helmholtz/Rayleigh-Taylor hybrid model," *Atomization and Sprays*, vol. 9, pp. 623-650, Nov-Dec 1999.

[21] Z. Y. Han, S. Parrish, P. V. Farrell, and R. D. Reitz, "Modeling atomization processes of pressure-swirl hollow-cone fuel sprays," *Atomization and Sprays*, vol. 7, pp. 663-684, Nov-Dec 1997.

[22] M. A. Patterson and R. D. Reitz, "Modeling the effects of fuel spray characteristics on diesel engine combustion and emission," 1998.

[23] Schmid, P.J., "Dynamic mode decomposition of numerical and experimental data", *J. Fluid Mech.* ,Vol. 656, 2010, pp. 5-28.

[24] Huang, C., Anderson, W.E., Harvazinski, M.E. and Sankaran, V., "*Analysis of Self-Excited Combustion Instability using Decomposition Techniques*", 51st Aerospace Sciences Meeting including the New Horizons Forum and Aerospace Exposition, January 07-10, 2013, Grapevine (Dallas/Ft. Worth Region), Texas.

[25] N. Syred, "A Review of Oscillation Mechanisms and the Role of the Precessing Vortex Core (PVC) in Swirl Combustion Systems," *Progress in Energy and Combustion Science*, Vol. 32, No. 2, 2006, pp. 93—161.

[26] N. Syred and J. M. Beer, "Combustion in Swirling Flows: a Review," *Combustion and Flame*, Vol. 23, 1974, pp. 143—201.

[27] Moses, C.A., "Comparative Evaluation of Semi-Synthetic Jet Fuels", Final report prepared for Coordinating Research Council, Inc. and Universal Technology Corporation.

[28] Rayleigh, J. "The Explanation of Certain Acoustical Phenomena", *Nature*, Vol. 18, 1878, pp. 319-321.

[29] Harvazinski, M.E., Huang, C., Sankaran, V., Feldman, T.W., Anderson, W.E., Mekle, C.L. and Talley, D.G., "*Combustion Instability Mechanisms in a Pressure-coupled Gas-gas coaxial Rocket Injector*", 49th AIAA/ASME/SAE/ASEE Joint Propulsion Conference, July 14-17, 2013, San Jose, CA